Research Article

Chemical reaction kinetics and the characteristic properties of injectable adhesives of nano-hydroxyapatite/Ag_3PO_4/polyurethane for bone and tooth repair

Quanjing Mei[1] · Lili Lin[1] · Jian Wang[1] · Bin Cai[1] · Qin Zou[1] · Jidong Li[1] · Yubao Li[1] · Yi Zuo[1]

Abstract
Advancements have been made to injectable polymer technologies following the development of minimally invasive techniques for bone and tooth treatment. To improve the conversion rate and avoid potential toxicity of traditional injectable polymer, new injectable adhesives have been developed to ensure good biocompatibility, while optimizing their suitable mechanical and antibacterial properties. In this study, we synthesized a two-part injectable n-HA/Ag_3PO_4/polyurethane system (PU) featuring different contents of nanohydroxyapatite (n-HA) and silver salt (Ag_3PO_4). After the prepolymer (Part A) mixed with a hardener (Part B), the compounded adhesive was injected into pores and set in situ with antibacterial properties. The results indicated that a high conversion rate reached 95% within 24 h could effectively reduce the release of a toxic monomer. Among these composites, the incorporation of n-HA in PU was the critical factor to ensure the adhesive's material characteristics and cytocompatibility. With the increased content of n-HA, from 0 to 30 wt%, the compressive strength, setting time, surface wettability, and differentiation activities improved significantly. Although the injectability and setting time of the PUs decreased with the increase of n-HA, the values of injectable PUs still met with ISO standard requirements. The antibacterial tests against *Staphylococcus aureus* showed that the incorporation of Ag_3PO_4 in PUs (1 wt% and 3 wt%) exhibited stronger antimicrobial effects than that without the addition of silver. Compared to the PUs with the addition of 3 wt% Ag_3PO_4, which led to poor cellular viability, PUs with 1 wt% Ag_3PO_4not only offered good antimicrobial properties, but also expressed excellent cytocompatibility, suggesting that this agent might be a promising injectable adhesive system.

Keywords Injectable adhesives · n-HA/Ag_3PO_4/polyurethane system · Reaction dynamics · Material characteristics · Antibacterial and cytocompatible properties

1 Introduction

Injectable adhesives offer significant advantages over preformed implants or autologous grafts, as the former can be administered using minimally invasive techniques while also conforming to irregularly shaped defects with a complex geometry [29, 42]. Among these adhesives, many injectable biomaterials in tooth repair have been used for bone fixation, and similar trends are likely to occur in clinic, such as the increased use of resin-based sealers and inorganic cements [13]. Early examples of synthetic adhesives include poly(methyl methacrylate) (PMMA) and related polymers, cyanoacrylates, lactide-methacrylate resin, glass ionomer cements, and calcium/magnesium phosphate cements [15, 56]. While polymeric adhesives have good mechanical properties, they often lack biocompatibility.

Electronic supplementary material The online version of this article (https://doi.org/10.1007/s42452-019-0707-x) contains supplementary material, which is available to authorized users.

✉ Yi Zuo, zoae@scu.edu.cn | [1]Research Center for Nano Biomaterials, Analytical and Testing Center, Sichuan University, Chengdu 610064, People's Republic of China.

SN Applied Sciences (2019) 1:746 | https://doi.org/10.1007/s42452-019-0707-x

Received: 9 January 2019 / Accepted: 3 June 2019 / Published online: 19 June 2019

Conversely, inorganic cements and fibrin-based resins have good biocompatibility, but the cohesive strength is insufficient for fixing defects of tooth and bone. Newer adhesive systems attempt to orchestrate multiple factors, including mechanical properties, cohesive strength, biocompatibility, and/or biodegradability, as based on clinical utility.

Recently, injectable adhesives based on polyurethane (PU) have become more promising than PMMA given their flexible molecular structure and low-reaction exotherm; PU injectable adhesives do not have hazardous effects on the surrounding environment [2, 12, 45]. Two-component injectable PUs have been prepared to explore potential orthopedic applications for bone-tissue repair [6]. Injectable and biodegradable lysine-derived PUs have also been studied, and no evidence of an adverse inflammatory response has been shown in femoral condyle defects in rabbits at 8 weeks [42]. However, there are still questions surrounding the clinical application of these PU adhesives. Bioreactive granules such as tricalcium phosphate (TCP) and bovine mineralized bone (BMB) have been dispersed in a catalyst solution before use or as a powder that is directly mixed with a viscous polymer and then cured, which resulted in nonuniform composites with unstable properties during polymeric network formation [42, 1]. Homogenous composition is the key factor when creating injectable biomaterials, as this forms a stable cross-linked network during the in situ setting process. A new injectable system of PU adhesives needs be explored.

Recently, we reported a high-conversion adhesive based on two-component reactive Pus [51]; however, pristine PUs have low biocompatibility for cellular infiltration and no radiopacity for clinicians' manipulation. Additionally, diffusion of water from the wound bed into the reactive PU can result in over-expansion of the polymer. When examining PUs in terms of their setting materials, proper storage expansion is preferred when they are used as adhesives to avoid radial pressure on the canal aspect, which may lead to a fracture of the root canal [28]. Inorganic fillers can increase the strength in, and control expansion of, the materials [42]. When compared to TCP and BMB granules, nanohydroxyapatite (n-HA) is a better candidate for inorganic fillers, as nanoparticles have good dispersibility, mobility, and bioactivity for injectable biomaterials [7, 32]. Herein, the incorporation of n-HA particles in urethane prepolymer is a more suitable technique that produces a homogeneous adhesive with enhanced properties in the injectable PU system [21]. In fact, uniform components and the stable properties of a reactive biomaterial are necessary features for commercially available materials. Besides these advantages, higher addition of n-HA also has some drawbacks such as brittleness and inferior curing property [11]. In this study, different proportions of the n-HA for PUs were synthesized to optimize the properties.

Injectable PUs meet another challenge for periprosthetic infection risk: irrespective of whether PUs are used for root canal fillings or bone fracture fixation in surgery, periprosthetic infections are possible, bacteria can adhere to the materials, making these infections difficult to manage and heal [35, 37]. An adhesive loaded with antibiotics may be useful for reducing potential risks associated with bacteria and enzyme penetration [39]. Many cements are supplied with antibacterial agents such as chlorhexidine, gentamicin, and tetracyclines, which target tooth and bone-repair infection. However, antibiotic resistance is the major contradiction of these antibiotics. Silver ions and silver compounds as broad-spectrum antimicrobial agents, have superior chemical and physical properties such as high thermal stability and low toxicity to human cells; as such, these agents can be applied in bactericidal products [43, 46, 54], including catheters, wound dressings, textiles, bone cements, and dental materials [3, 40]. In the former work of our laboratory, silver phosphate (Ag_3PO_4) has been introduced in PU materials, and it was found that the release of Ag^+ could provide satisfactory antibacterial effects [23, 53]. However, silver-loaded PU adhesives have low bioactivity for tissue repair. Researchers have found that excessive silver may result in unwanted adsorption of ions in epidermis cells and sweat glands [10]. Therefore, the effect of different contents of silver phosphate into PUs upon the antibacterial and cytocompatible properties was also investigated in this study. Cooperated with bioactive component of n-HA, a series of injectable PU systems have been studied to meet clinical requirements.

A self-adhesive formulation with good clinical feasibility, suitable mechanical properties, low toxicity, and good biocompatibility, and which also possesses the ability to prevent bacterial microleakage, is the ultimate goal among scientists, doctors, and companies in the realm of bone and tooth repair. As yet, the complexity and dynamics of the treating environment, as well as the high demands for materials with suitable mechanical and biological characteristics, mean that there are few commercial restorative materials that are ideal for all clinical situations [38]. A simple and controllable technique for adhesion assembly is thus needed to improve injectable systems.

In the present study, in view of high-viscosity PU materials, beneficial contents that include n-HA particles and silver components have been successively assembled in the reactive glues before a chain extender was added to compound a uniform viscous prepolymer effectively, known as Part A. Small molecular liquids and catalyst agents comprised a flowable hardener as Part B. Hand spatulation simplified the mixing condition for convenient clinic application. Based on this, mixed n-HA/Ag_3O_4/PU adhesives could

be injected in local sites of bone and tooth with bioactive compounds and improved antibacterial moieties.

The effects of nanoparticles and the antibacterial components of the injectable PU composites were investigated in this study to assess their reactivity and chemical reaction kinetics. The conversion rate of the isocyanate (NCO) group and the relative kinetic model of the composite adhesives during the curing process were calculated and deduced using reflection Fourier transform infrared (ATR-FTIR) spectroscopy. The chemical correlation between inorganic and polymeric components was investigated via the XPS spectra of representative samples. Moreover, the cross-linking structure of cured materials was quantitatively calculated based on its gel content and degree of swelling. For clinical applications, characteristic properties such as injectability and settability were evaluated according to ISO (International Standard Organization) 6876:2001. Meanwhile, the mechanical properties and hydrophilic performance of the surface was also tested for comprehensive evaluation of the nanocomposite adhesives. The drug delivery of silver ions and their antibacterial efficiency were evaluated in vitro. The cytotoxicity of the PU extraction solution during adhesive setting was tested according to ISO 10993-5:2009. Moreover, the proliferation and differentiation of mesenchymal stem cells (MSCs) on cured samples were assayed to discover the osteogenesis of PUs.

2 Materials and methods

Polytetramethylene ether glycol (PTMEG 2000), isophorone diisocyanate (IPDI), polyethylene glycol (PEG 600), and 2,2-Bis(hydroxymethyl)propionic acid (DMPA) were obtained from Shanghai Aladdin Co. Ltd. (Shanghai, People's Republic of China). Ag_3PO_4 was bought from J&K Scientific Ltd. (Beijing, People's Republic of China). Glutaraldehyde was obtained from Sigma-Aldrich Co. (St Louis, MO, USA). All reagents were of analytical grade. n-HA particles were synthesized via a wet chemical method and freeze-dried at − 50 °C according to our previous study [32] (TEM micrograph of n-HA is shown in the supplemental information in Fig. S1).

2.1 Prepolymer synthesis

2.1.1 Part A (prepolymer)

Pre-dried PTMEG2000 was weighed into a dry, three-neck flask equipped with a mechanical stirrer under a nitrogen atmosphere. IPDI was then added to the flask and the mole ratio of OH (PTMEG) to NCO (IPDI) was 1:1.2. The reaction mixture was stirred and heated to 70 °C for 5 h. Subsequently, different active moieties from the n-HA powder (0 wt%, 10 wt%, 20 wt%, and 30 wt%) and Ag_3PO_4(0 wt%, 1 wt%, and 3 wt%) were added, respectively, and the reaction was continued for 1 h. Then, DMPA as a chain extender was added into the flask because polyhydroxyl groups of DMPA can form the crosslinking with the -NCO groups of IPDI. Finally, the reaction ended and the NCO-terminated PU prepolymer was yielded as Part A.

2.1.2 Part B

Part B was obtained by mixing stannous octoate and polyethylene glycol homogeneously at the mole ratio of 1:15 at room temperature. Polyethylene glycol (PEG600) was pre-dried in a vacuum drying oven (100–120 °C) for 2 h before use.

2.1.3 Preparation of injectable PU composites

Injectable PU composites were obtained by mixing Part A with Part B. After the mixture of Part A and Part B, the mole ratio of NCO/OH for the whole reaction of PU was almost 1 to 1. By manually blending with a spatula for 30 s at ambient temperature, the mixture (which was the final PU-based adhesive) was immediately transferred to a 5 mL disposable syringe and then dispensed into a Teflon model (Φ6 mm × 12 mm) to produce cylindrical polymer samples. The samples in the mold were placed in an oven set at 37 °C to cure and then removed for additional testing. The cured PUs were named according to the details in Table 1.

2.2 Fourier transform infrared spectroscopy analysis

The Fourier transform infrared spectra (FTIR, Nicolet™ 6700, Nicolet Perkin Elmer Co., Waltham, MA, USA) was used to investigate the conversion during polymerization. Each sample was scanned 32 times with a resolution of 4 cm^{-1} in the range of 4000–500 cm^{-1}. The conversion rate of polymerization was calculated by comparing the peak area of the NCO group at different curing times.

Table 1 Compositions of the PU reagents

	0% HA	10% HA	20% HA	30% HA
0% Ag_3PO_4	PU00-0	PU10-0	PU20-0	PU30-0
1% Ag_3PO_4	PU00-1	PU10-1	PU20-1	PU30-1
3% Ag_3PO_4	PU00-3	PU10-3	PU20-3	PU30-3

The conversion degree of isocyanate, p, can be expressed by the following equation [30, 31, 53]:

$$p(t) = \int_0^t dp \tag{1}$$

where t represents the reaction time during the process.

Assuming that no side reactions occur, the isocyanate conversion (p) can be used as the degree of curing:

$$\text{Degree of conversion } (p) = 1 - \frac{A_t - A_\infty}{A_0 - A_\infty} \tag{2}$$

Here, A_0 is the integrated absorption area at the original time, A_t is the integrated absorption area at time t during the polymerization process, and A_∞ is the final integrated absorption area. Presuming no NCO groups will exist in the polymer, A_∞ is zero.

2.3 Physical and mechanical properties

2.3.1 Injectability and setting times

A mechanical testing machine (AGIC50 Shimadzu, Japan) was used to measure the injectability time of the samples using a compression rate of 20 mm/minute and the maximum force of 100 N according to ISO 6876:2001 [25, 38]. After mixing Part A with Part B for 30 s, the mixture was then placed into a 10 mL disposable syringe with an outlet at a diameter of 2 mm. The time required to reach the final force of 100 N was defined as the injectable time, and it was the equivalent of a function of the plunger travel time [44]. The extrusion set was processed at room temperature (25 °C).

The setting times of the various composites of the PUs specimens were assessed using Gillmore needles (453.6 ± 0.5 g) at room temperature according to ASTM (American Standards for Testing Materials) C266. According to this method, the setting time is the amount of time required for the test specimen to bear the Gillmore needle without appreciable indentation. When samples were mixed and injected into the mold, the setting time was tested according to the ASTM process. Tests were done in octuplicate.

2.3.2 Apparent density

Apparent densities of composites were determined from the mass and volume measurements of the samples from the Teflon model (Φ6 mm × 12 mm) and calculated using Eq. (3), where *m, d,* and *h*were the weight, diameter, and height of the specific PU samples, respectively.

$$\rho = \frac{4 \times m}{\pi \times d^2 \times h} \tag{3}$$

2.3.3 The degree of swelling

The degree of swelling (Q) of the network samples were tested via swelling experiments [52]. The cured PUs were swollen and extracted in alcohol for 48 h. By comparing the variations in sample weights before (the dry state m_d) and after (the swollen state m_{sw}) swelling, Q can be calculated by Eq. (4).

$$Q = 1 + \rho_2 * \left(\frac{m_{sw}}{\rho_2 * m_d} - \frac{1}{\rho_1} \right) \tag{4}$$

where ρ_1 is the specific density of the swelling medium and ρ_2 is the density of PU samples from Eq (3). Here, the swelling medium is dehydrated alcohol, where ρ_1 is 0.789 g/mL.

2.3.4 Gel content

The aforementioned 48-h immersed samples were dried in an oven (DZF 6090, Shanghai Yiheng Co. Ltd, Shanghai, People's Republic of China) at 60 °C for 24 h. The gel content (G) was the mass of the dried extracted sample (m_d) divided by the mass of the unextracted sample (m_{iso}).

2.3.5 Contact angle

The contact angle of the PUs was quantified by a Contact Angle Goniometer (JY-82A, Chengdu Dingsheng Testing Machine & Equipment Co. Ltd., People's Republic of China) through the sessile drop method at room temperature. Deionized water was dropped at five different locations with a micro-syringe on the surface of the composite samples. Then, the contact angle was analyzed using an image analysis system that calculated the contact angle from the shape of the drop.

2.3.6 Mechanical property tests

The compressive strength of the PUs was determined using a universal mechanical testing machine (AGIC Shimadzu, Japan). According to the ASTM standard D695-96, the composite samples were mixed and injected into a Teflon mold (Φ6 mm × 12 mm) and cured at 37 °C for 7 days before testing. The speed of the cross-head was 0.5 mm/minute and the load was applied until the specimen was compressed to approximately 40% of its original length. The experiments were done in quintuplicate.

2.3.7 XPS and EDS analysis

The chemical composition of the PUs was measured by X-ray photo electron spectroscopy (XPS). Data analysis was performed with the XPS Peak Fit 4.1 software. The molar concentration ratios were calculated from the peak areas (linear background subtraction), which were normalized based on the acquisition parameters. The C1 peaks were deconvoluted with a Lorentzian–Gaussian (20% of Lorentzian) product function. To compare pristine n-HA with n-HA composed in the PU matrix, PU20-0 was dissolved in dichloromethane to completely remove the polymeric material; then, the residual inorganic material was extracted and dried in a 37 °C oven for testing.

Scanning electron microscope (SEM JEOL 6500LV, JEOL, Tokyo, Japan) with an energy dispersive spectrometer (EDS INCA ENERGY 250, Oxford, UK) was used to characterize the structure and elemental distribution of the composites. The samples were sputtered with a thin gold layer prior to examination.

2.4 Ag^+ release behavior in the F12 medium

Quantitative analysis of Ag^+ release was measured by atomic absorption spectroscopy (AAS, SpectrAA 220FS; Varian, Palo Alto, CA, USA). The total concentrations of Ag^+ from PU30-1 and PU30-3 were assessed by dissolving 12.25 mm diameter, 1 mm thick disk-like samples in 10 mL of nitric acid, with a final load of Ag of 93.3 mg/L and 286.3 mg/L, respectively. F12 medium was used in the release of Ag^+ to obtain the cumulative release amount and release rate [55]. Each sample was weighed and immersed into a sealable tube containing 10 mL of F12. Three parallel samples were taken out at each time point (3 h, 12 h, 24 h, 3 days, 5 days, and 7 days) and the total release of silver ions was determined by AAS. The results were presented as the mean ± standard deviation (SD) for n = 3.

2.5 Antibacterial activity in vitro

The strain of bacteria used for this study was *Staphylococcus aureus*. The staphylococci were grown overnight in brain–heart infusion (BHI) broth (Oxoid Ltd, Basingstoke, UK) at 37 °C for 24 h until the exponential growth phase was reached. The inoculum density of 10^6 colony-forming units (CFUs)/mL was adjusted by spectrophotometric measurement at 600 nm and used for the antibacterial property assessment. All samples (Φ12.25 mm × 1 mm) of cured PUs were sterilized by autoclaving at 120 °C for 30 min.

2.5.1 Zone of inhibition

A total of 1 mL of the suspension (10^6 CFU/mL) was seeded slightly on the top of the culture dishes containing solidified nutrition agar; then, the sterilization samples were put in the middle of the culture dishes. After 24 h of incubation in a 37 °C incubator, the bacterial inhibition zone colonies were measured [17].

2.5.2 Bactericidal ratio

The 1 mL bacterial suspension (10^6 CFU/mL) was seeded on each of the samples in the tubes as the experimental groups. Then, 1 mL of bacterial suspension (10^6 CFU/mL) was added in the tube without a sample as the control group. The tubes were incubated at 37 °C for 24 h. At the end of the incubation period, the samples were gently rinsed for three times with phosphate buffered saline (PBS) to eliminate the non-adherent bacteria. After washing, the tubes were serially diluted in the range of 10^{-6} to 10^{-7}. Then, 100 µL dilutions were added in agar plates and incubated for another 24 h at 37 °C. After incubation, the number of colonies was observed and counted (Jones [24, 48]. The antibacterial effect in each group was represented by the bactericidal ratio, which was calculated as follows [36]:

$$\text{Bactericial ratio}(\%) = \left[\frac{\text{colonies of the control group} - \text{colonies of the experimental group}}{\text{colonies of the control group}}\right] \times 100 \quad (5)$$

Three replicate experiments were performed.

2.5.3 Antiadhesion assay

The sterilization samples were immersed in 1 mL of bacterial suspension (10^6 CFU/mL) and were incubated for 24 h at 37 °C. Then, the PU samples were gently washed with PBS to remove the unattached bacterial cells and were fixed with glutaraldehyde (2.5 vol %) for 2 h. Subsequently, the samples were dehydrated with gradient alcohol (30%, 50%, 70%, 80%, 90%, 95%, and 100%) and dried by the critical-point method. Finally, the freeze-dried samples were coated with gold and observed via SEM.

2.6 Cytocompatibility in vitro

2.6.1 Cell culture and seeding

To evaluate the biological properties of PUs in vitro, we focused on cell morphology and cell activity assays by direct contact with MG63 cells. The cells were routinely grown in F12 medium supplemented with a 10% volume fraction of calf serum, 1% penicillin/streptomycin, and 1% L-glutamine and maintained in a humidified incubator (37 °C, 5% CO_2). The media was replaced every 2–3 days. Following ultrasonic rinsing in distilled water and autoclave sterilization, the samples (Φ12.5 mm × 1 mm) were co-cultured with MG63 (2×10^4 cells/well) in a 24-well cell-culture plate (Corning, Corning, NY, USA) which were equilibrated in fresh medium (Gibco®; 1 mL/well) in a humidified incubator (37 °C, 5% CO_2) [58].

2.6.2 Cell morphology viability

The adhesion and morphology of MG63 cells growing on the cured PU samples were observed with SEM (JSM-6510LV; JEOL, Tokyo, Japan). Fixation in 2.5 vol% glutaraldehyde, dehydration through a graded ethanol (50%, 70%, 90%, and 100%), and drying of the critical point were carried out in situ. Afterwards, the samples were sputter-coated with gold before SEM observation [26]. Cell viability on the PUs was evaluated using the Live/Dead (viability/cytotoxicity) assay (Molecular Probes, Netherlands). After 7 days post-seeding, the samples were washed twice with PBS and incubated with Live/Dead solution (2 mol Calcein-AM and 4 mol ethidium homodimer) at room temperature in the dark. After combination dying for 30 min and after being washed twice with PBS, the samples were subsequently analyzed with an inverted microscope (TE2000-U, Nikon, Japan) with a 100 W Hg lamp and photographed. The viable cells (in green) and nonviable cells (in red) were distinguished under the fluorescence microscope [47].

2.6.3 Cell cytotoxicity and proliferation

The cytotoxicity of the PU30 series was tested by examining the MG63 cells by CCK-8 (Sigma-Aldrich Co.), an assessment that was carried out according to ISO 10993-5. Cured PU30-0 s, PU30-1 s, and PU30-3 s were cut into blocks immersed in F12 medium supplemented with 10% volume fraction of calf serum for 24 h at 37 °C in the humidified atmosphere of 5% CO_2 and 95% air. The surface area-to-volume ratio is 3 cm^2/mL. After incubation, the extraction was filtrated for use. Concentration gradients of 12.5%, 25%, 50%, 75%, and 100% were used as experimental groups. Pristine F12 medium (0% extraction) was used as the blank control group. Then, 100μL of F12 medium was added in 96-well plates and incubated at 37 °C overnight for pre-soaking. The medium was then removed and replaced with 100 μL of a cell suspension at a density of 5×10^3 cells/well. The 96-well plates were cultured in a humidified incubator (37 °C, 5% CO_2) for 24 h and then replaced by extraction. The extraction was changed every 2 days. At each point (1, 4, and 7 days) 10 μL of CCK-8 solution was added into each well. After 3 h of incubation, absorbance was measured at 450 nm. The cell viability expressed by a relative growth rate (RGR) was calculated using the average absorbance of the samples (OD_{sample}) divided by the absorbance of the control groups (OD_{blank}). Five samples per group were measured to obtain a mean value.

2.6.4 Cell differentiation

MSCs were obtained from the femurs and tibiae of Sprague–Dawley rats with a weight of approximately 100 g. The alkaline phosphatase (ALP) activity of MSCs cultured for 7 days and 14 days were assayed using the Rat ALP ELISA Kit. MSC cells were seeded at a concentration of 2×10^4 cells/well in the 24-well plastics. At each time, the culture medium was abandoned and the remaining cells were lysed with 0.2% Triton X-100. After 5 min of centrifugation, the lysate was collected for the ALP activity test according to the manufacturer's protocol and the optical density (OD) was measured at 450 nm. The cells were counted before lysis using a cell counter.

2.7 Statistical analysis

Data were collected in a Microsoft Excel 2010 database and filtered using a Box Chart of the Origins 9.0 software. Valid data were presented as the mean ± standard deviation (SD). Statistical analysis was calculated using the Graphpad InStat software (InStat® 3.0, Graphpad Software Inc., La Jolla, CA, USA). The statistical analysis was carried out using one-way analysis of variance (ANOVA) with Tukey's test for multiple comparisons, $P < 0.05$, indicating statistical significance.

3 Results

3.1 Effect of beneficial constituents in the injectable PUs

Polymeric nanocomposites have attracted sought-after interests because of their improved properties when compared to the constituent parts, design flexibility, and uniquely large applicability in various clinical fields. Nanoparticles dispersed inside the polymer matrix is the

advanced function of the produced material. As a result, the PU prepolymers combined suitable properties of both partners in this study, of which bioactive n-HA combined with silver salts have been used as functionalizing agents. Numerous nanoparticles require well entrapment on substrates and matrices for unique physicochemical, biological, and antimicrobial properties [10]. From this point of view, the specific morphology, as well as the chemical and structural nature of the injectable nanocomposites have been investigated to discover whether functional constituents incorporated and fine dispersed in the long polymeric chains form a unique injectable material.

The prepolymerization reaction of Part A was described as follows. First, the hydroxyl groups of PTMEG as a proton donor copolymerized with aliphatic IPDI. Then, DMPA as a chain extender was added. IPDI and DMPA formed the hard segment of the preplomer molecular chain, while PTMEG formed the soft parts. Finally, n-HA and Ag_3PO_4 were added with different proportions. In all cases, a mild reaction between –NCO (in Part A) and –OH (in Part B) proceed after mixing Part A and Part B. The homogeneous mixture could be injected to the desired location and was cured at body temperature. EDS maps, FTIR, and XPS spectra were analyzed in this section to reveal the distribution and interfacial bonding of n-HA in the PU matrix. The EDS micrographs in Fig. 1a showed a uniform dispersion of Ca, P, and Ag elements in the PU matrix. Few large aggregates of the three elements were observed from the images.

The influence of beneficial constituents on polymerization was investigated by tracing the chemical changes and chemical state with FTIR and XPS techniques. Figure 1b showed the representative FTIR spectra of reactants, prepolymers, and cured PUs (the FTIR results of all groups are shown in the supplemental information in Fig. S2). Most of these characteristic peaks were consistent with those in previous reports for n-HA and PU, respectively [33]. We confined our attention to the spectral changes that appeared in the polymerized and cured process of injectable PU nanocomposites. Peaks at 1,719–1,723 cm^{-1} emerged in all prepolymers and cured materials, which were attributed to the stretching vibration of carbonyl (C=O) groups, meaning that the urethane groups formed during polymerization. On the other hand, the characteristic bands, e.g. the intensity of the OH envelope peak

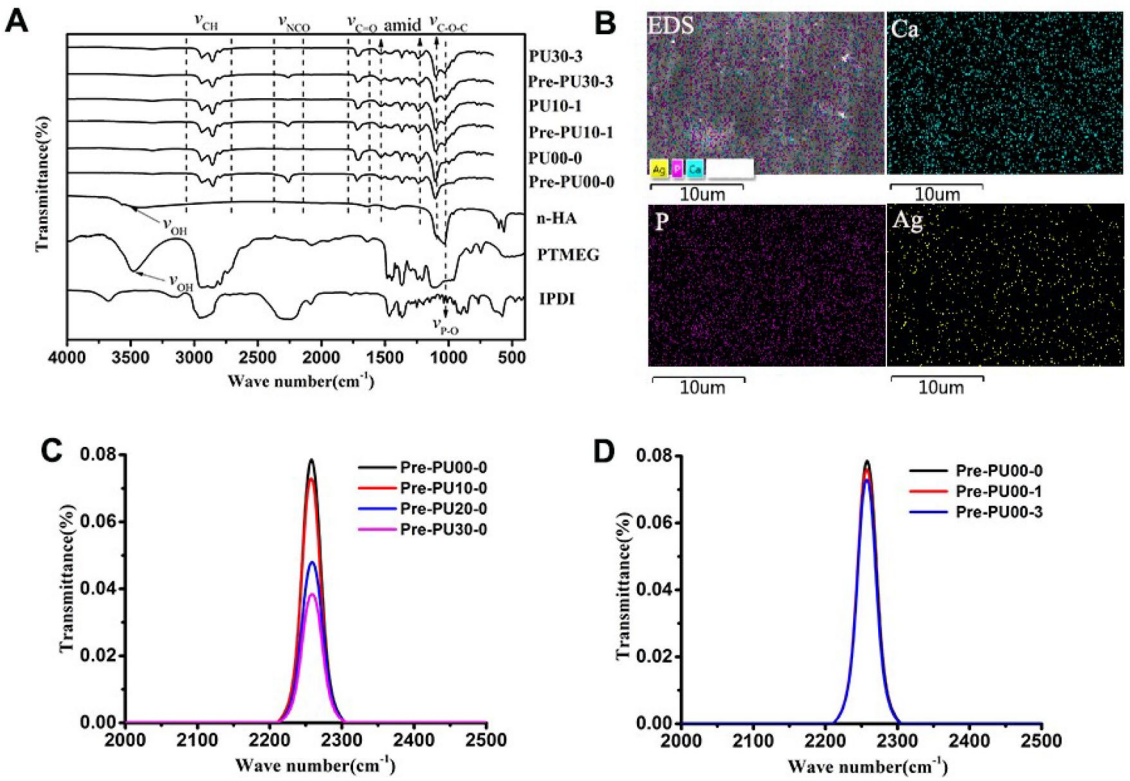

Fig. 1 **a** FTIR spectra of IPDI, PTMEG, n-HA, pre-PUs, and PUs cured for 24 h at 37 °C. Complete polymerization of cured PUs was observed by the disappearing peaks of the NCO groups at 2259–2261 cm^{-1}. **b** EDS mapping of the cured PU30-3 with the uniform distribution of Ca, P, and Ag elements. **c** The density of the NCO groups at 2,260 cm^{-1} of the pre-PUs was largely influenced by the different n-HA contents; **d** the density of the NCO groups at 2260 cm^{-1} of pre-PUs was weakly affected by different sliver contents

around 3,500 cm^{-1}, of PTMEG disappeared and the –NCO stretching vibration at 2259–2261 cm^{-1} of IPDI decreased sharply, which indicated that the free OH and NCO groups reduced drastically during the synthesized procedure. Further, the relatively high intensity of the NCO groups in the pre-PU sealers depicted that Part A was an NCO-terminated prepolymer. Subsequently, the peaks of the NCO groups completely disappeared after mixing Part A with Part B; this can be attributed to the sufficient polymerization that occurred to form the final products (PU00-0, PU10-1, and PU30-3). The peaks at 1094 cm^{-1} and 1030 cm^{-1} (P-O stretching of the PO_4 groups) and 875 cm^{-1} (P-O stretching of the HPO_4^{2-} groups) suggested the presence of the HA phase in the composite.

Typical change of the FTIR peaks at 2,260 cm^{-1} for the NCO groups was affected by the addition of n-HA particles in Part A (Fig. 1c). Without the addition of a sliver reagent, the intensity of the NCO groups decreased significantly with the increase of HA contents. It should be noted that the intensity of pre-PU00-0 was twice as high as that of pre-PU30-0; however, little influences have been observed while the content of Ag_3PO_4 increased (Fig. 1d). Similar changes were observed for other contents of HA and sliver (Fig. S2).

An analysis of the XPS data provides insight into the local oxidation states and chemical bonding environment of the composed materials using subtle changes in peak positions and shapes. To further investigate the elements present and their chemical states (valence) for polar n-HA and the amphiphilic PU matrix, the deconvoluted XPS C1 s spectra for PUs and HAs were resolved into three characteristic peaks, as shown in Fig. 2a–d. C1s binding energies at peak position and at the peak area, as calculated from the fitting curves of the XPS spectra, were displayed in the upper-right corner of the images. The observed deconvoluted peaks at 284.66–284.8, 286.03–286.09, and 288.19–288.91 are to the functional groups of C–C, C–O, and C=O, respectively. With the incorporation of n-HA, the peak position for binding energy of C=O shifted from 289.19 eV to 288.86 eV and the peak area of C=O (HN–CO–O group) increased from 1.24 to 3%, as shown in Fig. 2a–b. The shift of the carboxyl peak to a lower binding energy should be attributable to the specific bonding of n-HA and the PU matrix. At the same time, the wide-scan XPS spectra and deconvoluted C1 s spectra of pristine n-HA and n-HA extracted from pre-PU20-00 were shown in Fig. 2c–e. An obvious N-peak was observed in the spectrum of n-HA extracted from pre-PU20-00, while no N peak was shown in that of pristine n-HA (Fig. 2e). Furthermore, the intensity of the C and O peaks decreased significantly, and the intensity of the Ca and P peaks increased in the extracted n-HA spectrum (Fig. 2e). The deconvoluted XPS spectrum of C1 s in extracted n-HA (Fig. 2d) showed an obvious C–O peak similar to that of pre-PU20-00 (Fig. 2b), but the peak did not exist in pristine n-HA (Fig. 2c). Moreover, the peak position for the binding energy of C=O shifted from 288.38 to 288.91 eV when compared with pristine n-HA (Fig. 2c).

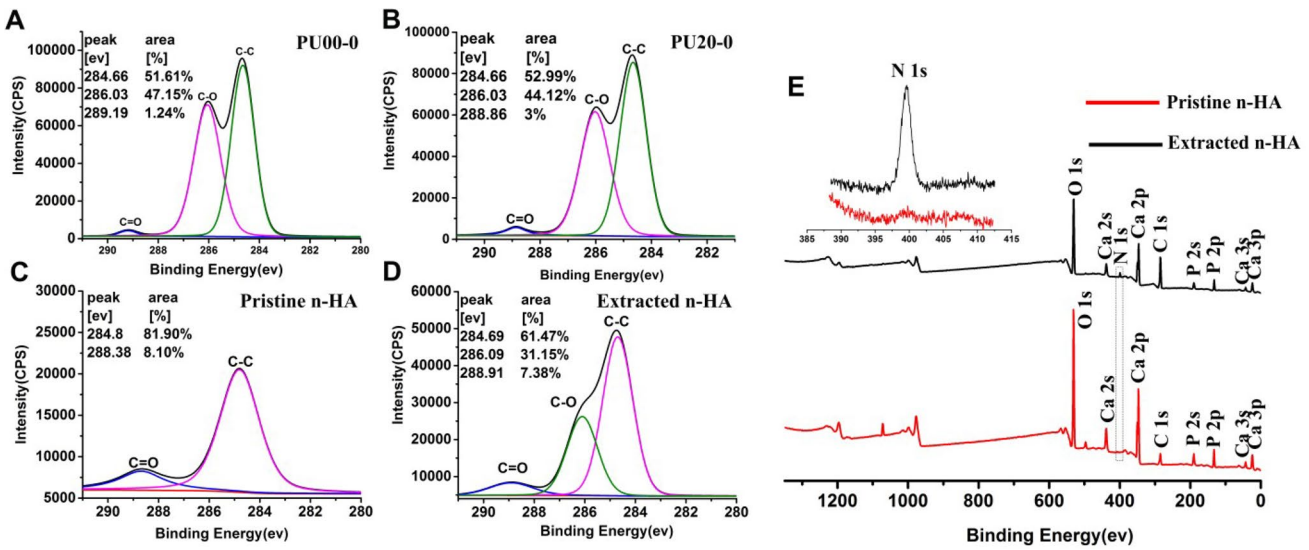

Fig. 2 The deconvoluted C1 s XPS spectra for PU 00-0 (**a**), PU 20-0 (**b**), pristine n-HA (**c**), and n-HA extracted from pre-PU20-00 (**d**) to analyze the interfacial interaction between the added nanoparticles and polymeric matrix. Note the shift of the carboxyl peak (C=O) to a lower binding energy from (**a**) to (**b**). An obvious C-O peak was observed in the extracted n-HA, which was similar to pre-PU20-00, but it did not exist in pristine n-HA. **e** The wide-scan XPS spectra for pristine n-HA and n-HA extracted from pre-PU20-00. An N peak was observed in the spectra of n-HA extracted from pre-PU20-00

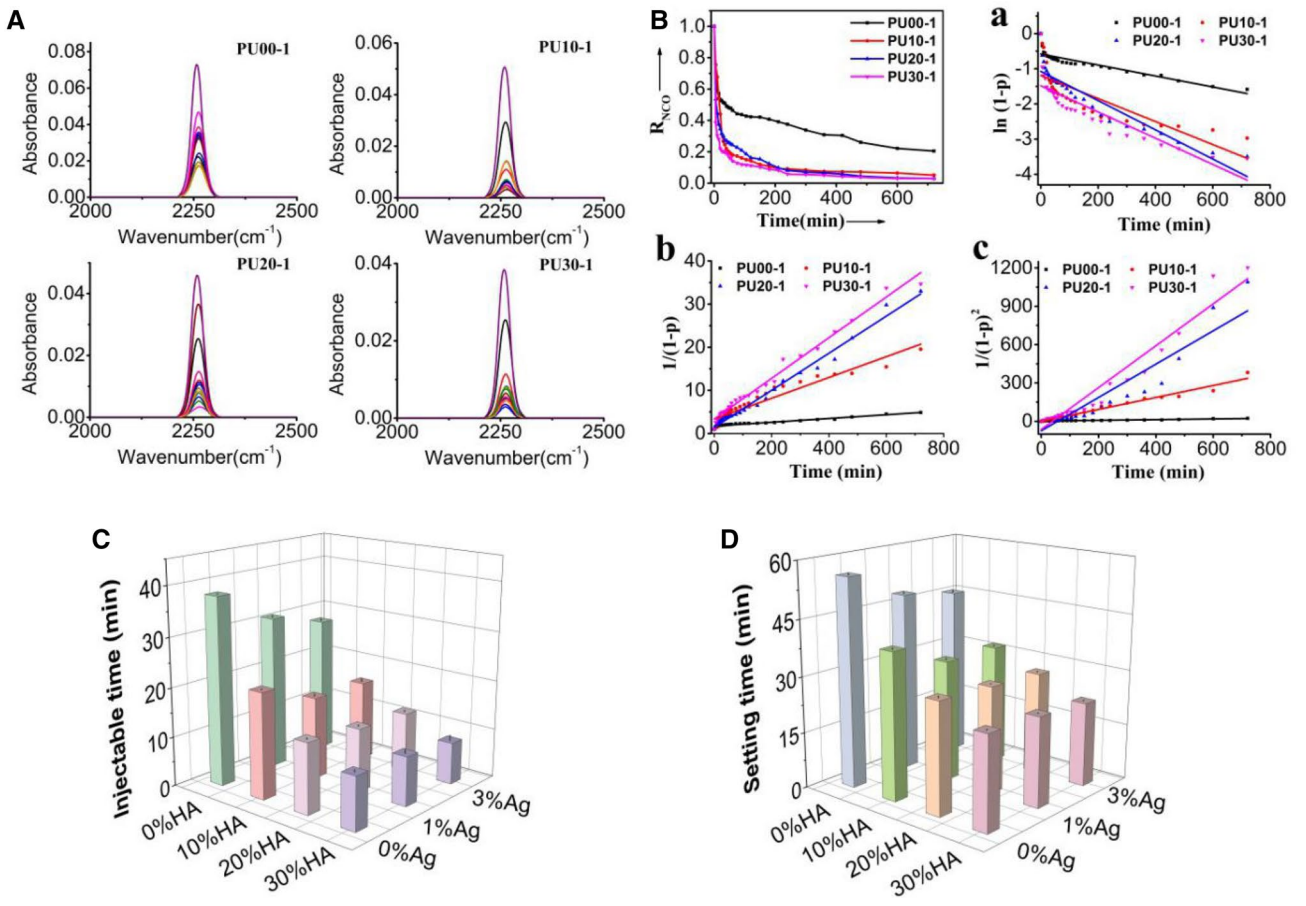

Fig. 3 **A** The representative NCO peak of FTIR spectra of PUs with cure time (0, 5, 10, 15, 20, 25, 30, 35, 40, 45, 50, 55, and 60 min); **B** The integrated –NCO peak area versus time and the relationship between p and curing time of PUs when the reaction order is (a) $n=1$; (b) $n=2$; and (c) $n=3$. **C** Injectable time and **D** setting time of the PUs

Meanwhile, the influence of beneficial constituents on polymerization were investigated by tracing the chemical change at different treatment times by using in situ reflection FTIR techniques. Figure 3A, B illustrated representative FTIR spectra of PU00-1, PU10-1, PU20-1, and PU30-1 (the FTIR results for all groups are shown in supplementary Fig. S3). Figure 3A showed that the absorption spectra of NCO decayed after increasing the curing time once Part A mixed with Part B; the reactions of the PUs demonstrated a similar tendency in all formulations. At the first 10 min, the PUs reacted rapidly and consumed about 50% of the content of the NCO groups. Subsequently, the conversion of NCO decreased slowly after increasing the curing time. After 60 min, 90% of the NCO groups participated in the curing reaction, except for PU00-1, which had the lowest degree of monomer conversion.

The integrated peak areas were calculated and listed in Fig. 3B to evaluate the conversion that qualitatively changed over time. Figure 3B also showed that the addition of n-HA particles could considerably enhance the polymerization procedure of PUs. For example, the data indicated that about 20.5%, 5.1%, 2.7%, and 1.9% of the NCO groups remained in PU00-1, PU10-1, PU20-1, and PU30-1 after 12 h, respectively. In addition, the degree of NCO conversion for all PUs reached 95% after 24 h of curing.

According to empirical rate laws, the conversion degree can be expressed as a function of curing degree and temperature [30, 34]. The curves in Fig. 3Ba–Bc are results calculated by three different order equations (listed in the supplemental information) applied to the curing process. Based on the equations, the curves and fitting results of all experiment groups in Fig. S4a–S4c were calculated and summarized in Table S1 in the supporting data. From the specific curves of the non-sliver samples, it is evident that only the curing process for PU00 s was more supported in the third-order reaction, while the other samples of PU10 s, PU20 s, and PU30 s were more supported in the second-order reaction.

3.2 Characterization of adhesive properties

3.2.1 Injectability and setting time

Injectability and setting time are the key characteristics in the application of injectable adhesives [31]. As per Fig. 3C, D, the average injectable time decreased from 37.9 to 27.7 min when the Ag_3PO_4ratio increased from 0 to 3 wt%, of which the reduced ratio was 26.9%. Furthermore, the average injectable time decreased from 37.9 min to 10.7 min when the n-HA ratio increased from 0 to 30 wt%, of which the reduced ratio was 71.8%. With the increase of the inorganic phase, it became more difficult to extrude the mixtures, so that the injectable time was faster to reach the final force of 100 N. However, the difference in injectable time caused by the Ag_3PO_4 concentration became much less than the change caused by the increase of n-HA contents. The final setting time had the same changeable tendencies with injectable time. The average setting time decreased from 55.8 to 45.5 min (reduction: 18.5%) when the Ag_3PO_4 ratio increased from 0 to 3 wt%. Further, the average setting time also greatly decreased from 55.8 to 22.9 min (reduction: 59.0%) when the n-HA ratio increased from 0 to 30 wt% (the specific injectability and setting time values are displayed in supplemental Table S2).

3.2.2 Physical and mechanical properties

Since the PU adhesives are injected as low-viscous slurries and are transformed in the body to a solid, cross-linking is a crucial property for the gel formed in situ. Here, the cross-linking density of the PU networks can be extracted from swelling and gel content. As per Table 2, all PUs had a high gel content of above 96% and the incorporation of n-HA and Ag_3PO_4 nanoparticles did not significantly reform the gel. As for the degree of swelling, which depends on the cross-linking density of the polymer network, the values decreased significantly with increasing n-HA. The apparent densities of each PU sample (Table 1) rose from 0.993 g/cm^3 (PU00-0) to 1.177 g/cm^3(PU30-3); however, no significant difference was observed.

The data in Table 2 indicated a positive effect of the n-HA particles on the compressive properties of PUs. When the n-HA particles were incorporated into the polymer matrix harmoniously, the compressive strength of the PU30 s increased significantly up to 3.850 MPa, which was about 2.5 times higher than that without n-HA of 1.521 MPa (PU00-0). However, the doping of Ag_3PO_4 to the PUs did not seem to change the compressive strength during polymerization. With respect to the surface property, the contact angle of PU00 s was around 79° ~ 80°, while the lower contact angle of 70° ~ 72° was measured by the incorporation of HA nanoparticles (Table 2). Similar to compressive strength, no significant changes were observed in the contact angles of PUs with increasing Ag_3PO_4 content.

3.3 Antibacterial property testing in vitro

Although silver is probably the most powerful antimicrobial agent that exhibits strong toxicity toward a broad range of microorganisms, its use may result in unwanted adsorption of ions in epidermis cells and sweat glands [10]. The observed toxicity has been assigned to the oxidation of the surface ions toward silver cations that can affect basic cellular functions in mammalian cells [22]. From this point of view, the immobilization of silver ions on PU substrates seems advantageous for less direct

Table 2 Physical and mechanical properties of PUs

Sample	Gel content (G, %)	Degree of swelling (Q, %)	Apparent density (g/cm^3)	Compressive strength (MPa)	Contact angle (degrees)
PU00-0	98.131 ± 1.530	168.442 ± 6.584	0.993 ± 0.003	1.521 ± 0.18	80.292 ± 2.526
PU10-0	98.469 ± 0.382	147. 282 ± 0.562***	1.050 ± 0.002	2.303 ± 0.33**	78.946 ± 5.561
PU20-0	98.125 ± 0.146	141.002 ± 1.621***	1.094 ± 0.002	2.794 ± 0.25**	74.398 ± 3.19**
PU30-0	98.069 ± 0.131	137.468 ± 0.982***	1.127 ± 0.004	3.206 ± 0.32***	70.233 ± 4.227***
PU00-1	98.354 ± 0.141	167.442 ± 6.655	1.045 ± 0.011	1.443 ± 0.078	79.105 ± 3.024
PU10-1	97.955 ± 0.108	146.599 ± 2.119***	1.074 ± 0.004	2.778 ± 0.470**	77.105 ± 4.61
PU20-1	97.301 ± 0.491	140.301 ± 2.569***	1.131 ± 0.009	3.092 ± 0.577***	74.455 ± 4.520
PU30-1	97.189 ± 0.329	137.213 ± 2.127***	1.176 ± 0.055	3.850 ± 0.624***	72.740 ± 4.651**
PU00-3	97.714 ± 1.239	163.264 ± 6.653	1.041 ± 0.011	1.350 ± 0.099	79.026 ± 4.004
PU10-3	96.874 ± 2.130	145.699 ± 1.217***	1.057 ± 0.001	2.787 ± 0.056***	74.906 ± 2.539
PU20-3	96.364 ± 0.083	141.316 ± 1.029***	1.135 ± 0.018	3.077 ± 0.298***	72.258 ± 3.313**
PU30-3	96.167 ± 0.200	135.919 ± 1.451***	1.177 ± 0.015	3.221 ± 0.187***	71.183 ± 1.065***

*Denotes significant difference from the PU00s, *$p < 0.05$, **$p < 0.01$, ***$p < 0.001$

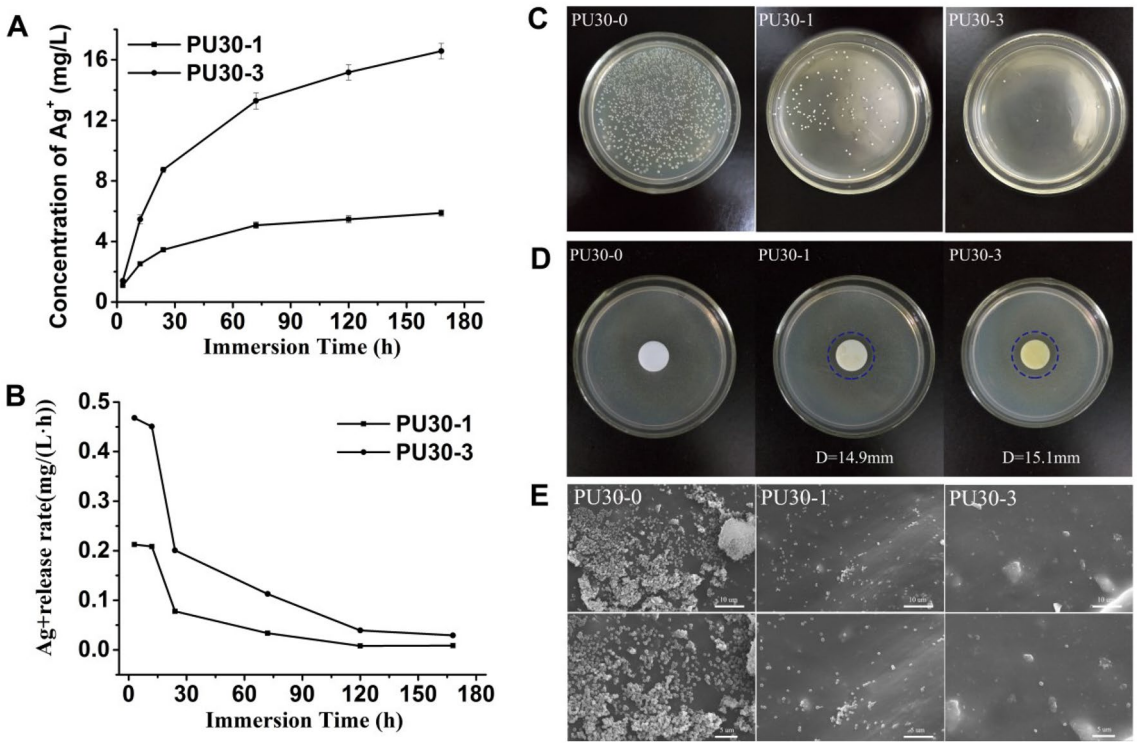

Fig. 4 **a** Concentration of silver ions released from PU30-1and PU30-3 in the F12 medium in time-course tests; **b** Ag^+ release rate against time in F12 medium. **c** Photos of bactericidal ratio testing, **d** Inhibition zone test and **e** SEM images of bacterial adhesion of the PU30 s with different Ag_3PO_4 contents against *S. aureus* after 24 h of incubation

uptake of the particles from mammalian cells than the silver particles. First, the release behavior of Ag^+ and the antibacterial properties of the samples were tested as the functional and beneficial assessment of PUs.

3.3.1 Ag^+ release behavior in the F12 medium

The concentrations of Ag^+ released from the PUs in the F12 medium over time are shown in Fig. 4a. The amount of Ag^+ released had increased with increasing concentrations of Ag_3PO_4 content in the PU samples, and the curves were somewhat parabolic. In addition, the concentration of Ag^+ quickly released in the first 3 days, at which point the release values progressively slowed. Approximately 5.4% and 4.6% of Ag^+ were released from PU30-1 and PU30-3, respectively, within the first 3 days. There was still about 93.7% and 94.2% of Ag in PU30-1 and PU30-3 at the final testing point of 7 days. The curves of the release rate over time are shown in Fig. 4b. The release rate of Ag^+ decreased rapidly after initial immersion until 24 h, at which point the release rates began to slow until 5 days; finally, the rates leveled off and reached equilibrium within the last testing stage.

3.3.2 Antibacterial testing

The antibacterial testing results for various Ag_3PO_4 contents of PU30 s are shown in Fig. 4c–e. With the increase in Ag_3PO_4concentrations, the number of colonies decreased significantly (Fig. 4c). Almost no bacterial colonies were observed on the PU30-3 plate. The bactericidal ratios of PU30-1 and PU30-3 calculated by Eq. 6 with PU30-0 as the control group were 93.09% and 99.55%, respectively. No inhibition zones were observed on the silver-free PU30-0; however, PU30-1 and PU30-3 had an obvious zone of inhibition with diameters of approximately 15 mm (Fig. 4d). Similar results were observed in the SEM analysis of the antiadhesion assay (Fig. 4e). The antiadhesive ability against *S. aureus* was strengthened with the increase of Ag_3PO_4 incorporation. Just a few bacteria were observed on the surface of the PU30-3 samples.

3.4 Cytocompatibility evaluation in vitro

To evaluate the cytotoxicity and bioactivity of PUs that carried Ag_3PO_4 and n-HA, different types of tests have been used based on different sample processing techniques. Cytotoxicity was monitored by CCK-8 analysis to

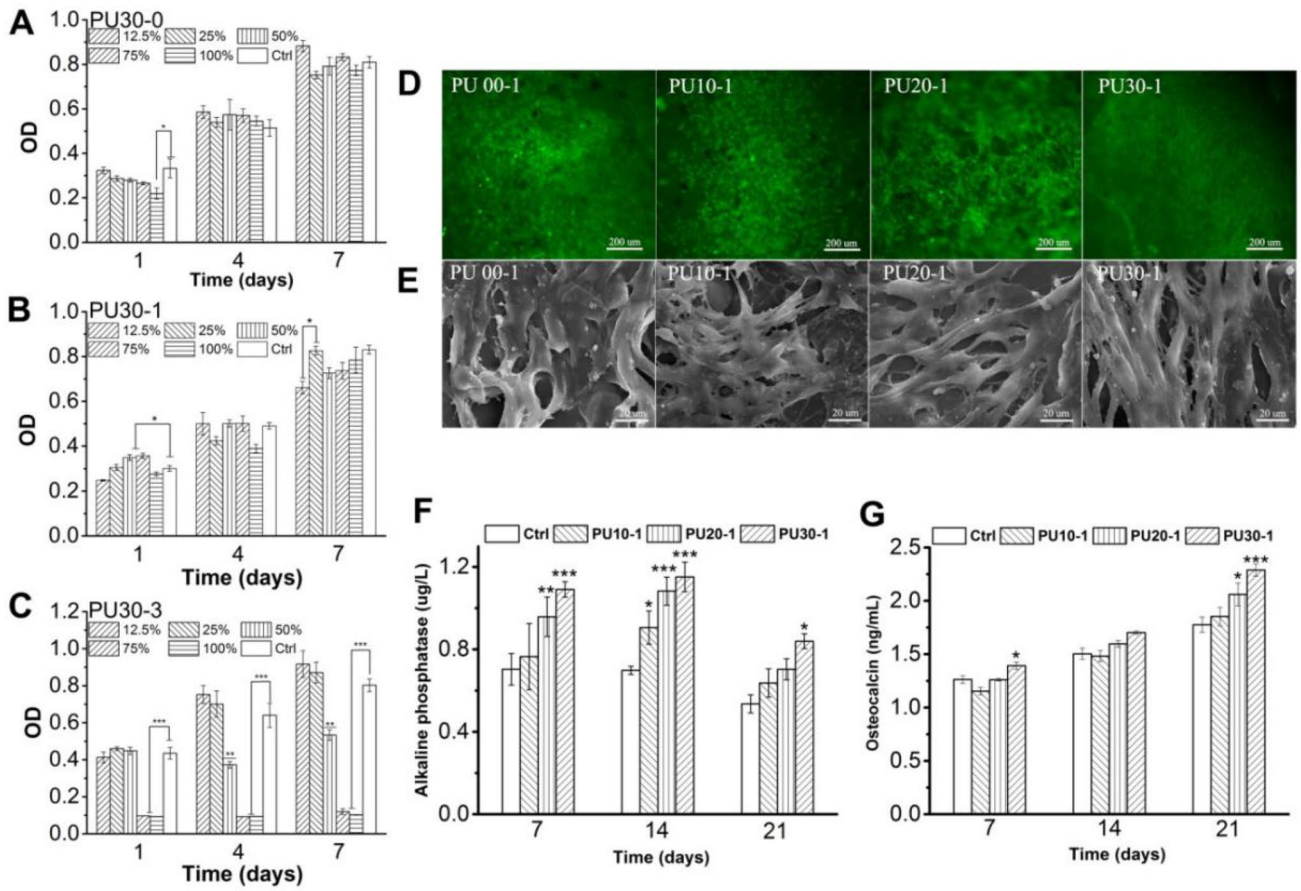

Fig. 5 The OD values in CCK-8 tests after culturing in extracts of PU30 s with different content for different periods. **a** PU30-0, **b** PU30-1, **c** PU30-3. **d** The fluorescence images and **e** SEM photographs of MG63 s cultured with PUs for 7d. **f** ALP activity and **g** OCN assay of MSCs cultured with PUs for 7, 14 and 21 days compared with the blank control (tissue culture plastic) for the same culture condition Error bars represent the standard deviation from the mean ($n = 5$); *** $p < 0.001$, ** $p < 0.01$, * $p < 0.05$

assess cell proliferation using MG63. Figure 5a–c demonstrated the *OD* values of the CCK-8 test after 1 day, 4 days, and 7 days of incubation at gradient extracting concentrations. For the PU30-0 and PU30-1 samples, the OD values did not exhibit a significant difference with the control group, except for a few extracted concentrations (Fig. 5a, b). However, the OD values of PU30-3 presented a statistically significant difference with the control groups in higher concentrations of 50%, 75%, and 100% extracts, meaning that the silver content in the composites significantly impacted cytotoxicity.

According to ISO 10993-5: 2009, these RGR results were mostly ranked as grade 0 (RGR: 90%–100%) and grade 1 (RGR: 75%–90%). Generally, grade 0 and grade 1 were not supposed to be toxic to the cells. Here, 75% and 100% of extracts of PU30-3 were ranked as grade 3, which were considered to be severely toxic to cells.

The morphologies of MG63 PUs co-cultured for 7 days were shown in Fig. 5d, e. In the live/dead staining images shown in Fig. 5d, the cells exhibited a normal and healthy polygonal shape and limited intercellular communication. From the SEM results in Fig. 5e, it was clear that a mass of cells adhered and fused to a layer on the surface of the PUs with numerous filopodia, lamellipodia, and cytoplasmic extensions. Cell viability was not affected by the increase of n-HA incorporation.

Being an early marker, ALP plays a crucial role in recognizing the initiation of the mineralization process by cell differentiation. Figure 5f showed the ALP activities of MSCs cultured on different PUs. During the culture period from 0 to 21 days, the ALP activity maintains a relatively high value at 7 and 14 days, and it then decreases up to 21 days. Further, with increasing concentrations of n-HA, ALP activities increased much higher when compared to the control groups, especially on day 14. A significant difference between the control group and the PUs was observed on day 14. Osteocalcin (OCN) is generally considered to express at the middle-to-later

stages of MSC differentiation. The OCN expression in Fig. 5g showed trends of an increase with the increase of culture time; maximum expression was evident on day 21. Meanwhile, high OCN values of PUs with30% n-HA confirmed the statistically positive effect of n-HA toward osteogenic differentiation.

4 Discussion

In this study, we developed a two-component, self-curing PU system for injectable adhesives based on the reaction between IPDI and PTMEG. Different contents of n-HA and Ag_3PO_4 were incorporated to increase the positive functions, which included material characteristics, cytocompatibility, and antibacterial properties.

4.1 Chemical reaction kinetics and physicochemical properties

The results of FTIR and XPS analysis demonstrated that n-HA particles had bonded with the PU matrix. From the FTIR results, the primary OH groups of the n-HA particles reacted with the NCO groups of IPDI and appeared to result in attenuation of the peak of the NCO group (Fig. 1c). Since FTIR cannot reveal indisputable evidence of chemical bonding of the PU matrix with n-HA, XPS was selected to sensitively detect the chemical bonding between n-HA and PU at the interface. The appearance of the N peak and changes of the relative peak intensity of the Ca, P, and C elements indicated that these elements were the major constituents of PU nanocomposite systems (Fig. 2e). Meanwhile, the red shift of C=O excluded the simple adhesion of PU on n-HA, but it connected with n-HA through chemical bonding (Fig. 3A–D). Figure 6 presents the schematic diagram of the principle of postulated chemical bonding between the inorganic–organic intermolecular interaction. The formation of PU composites is dominated by reaction 1 and the incorporation of n-HA introduced reaction 2 (Fig. 6A). The intermolecular bonding between the OH groups of n-HA and the NCO groups of IPDI offset the electron pairs and resulted in a reduction of the bonding energy of C=O from 289.19 to 288.86 (Fig. 2a, b). The formation of chemical bonding was more stable than simple physical blending and this contributed to a stronger inorganic–organic interface bonding and to a more robust intermolecular interaction [20]. Consequently, the n-HA particles with uniform dispersity (presented in Fig. 6b) chemically bonded with the NCO groups on the polymer chains, which strengthened the mechanical strength and promoted the conversion rate of the PUs.

The incorporation of n-HA resulted in a significant increase in the reaction and conversion rates, which could be due to the reaction between NCO-terminated pre-PU and hydroxyls of n-HA particles, as discussed earlier. This reaction

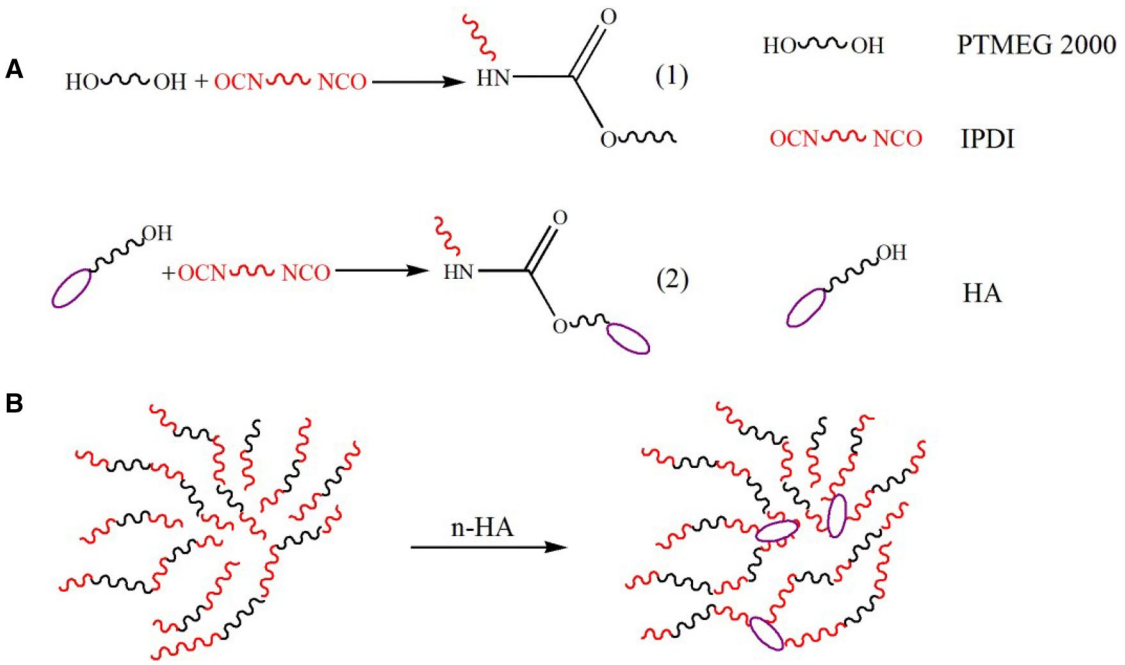

Fig. 6 **a** Schematic of the chemical bonding between the OH groups and NCO groups of IPDI (1) pure PU and (2) n-HA addition; **b** Schematic of n -HA particles, which were uniformly dispersed in the polymeric matrix

brings about a phenomenal decrease in the NCO peak in Part A (Fig. 1c). In view of the nearly null influence resulting from the addition of the silver reagent (Fig. 1d), the polymerization mechanism and kinetics had correspondingly changed in response to the n-HA particles during the self-curing process. The polymerization kinetic studies were focused on the addition of n-HA. In addition to the bonding reaction between the OH groups of n-HA and the NCO groups of PU, it was found that the n-HA particles also improved higher viscosity in the system, with more content of inorganic filling, thus accelerating the polymerization process [20, 33]. Consequently, the curing process of PUs without n-HA supported the third-order reaction, but the process of PUs with the addition of n-HA were in agreement with a second-order reaction, which fasts the setting process; this is why PU10 s, PU20 s, and PU30 s had higher reaction rates and conversion ratios. The high conversion ratio of the NCO groups did not only avoid cytotoxicity [19, 53] by decreasing residual free monomers during polymerization, but they also resulted in more favorable mechanical properties by the formation of interpenetrate polymer networks [18, 51]; these properties included surface hardness, compressive strength, and fracture toughness. Therefore, the setting time and surface contact angle had reduced, and the compressive strength increased with higher concentrations of n-HA (Fig. 3c–d; Table 2). Since the reaction was controlled by different factors during different procedures, this kinetic approach was not suitable for evaluating the entire curing process. In fact, the entire curing process can be divided into three parts. At the beginning, the rate was dominated by the reaction between isocyanate groups from Part A, as well as by the hydroxyl groups from Part B. The stick adhesives transformed into gel by chemical cross-linking. After completing consuming the active groups of Part B, the rate was controlled by the reaction between isocyanate groups and hydroxyl groups from the environment. At the end of the polymerization reaction, the flowable gel gradually became solid. Ultimately, the reaction rate was controlled by mild diffusion in situ, rather than by fast chemical bonding. The incorporation of n-HA particles decreased the injectable and setting times significantly given the high reaction rate and convert ratio. Conversely, the slight changes of the injectable and setting times caused by the Ag_3PO_4 (Ag^+) may be attributed to the positive catalytic effects on polymerization [53]. The long setting time is an urgent problem for surgical application. It was reported that Kryptonite™, a United States Food and Drug Administration (FDA)-approved PU bone adhesive, requires 24 h' fixation time [16]. Rather, a quick setting time of about 0.5 h ~ 1 h of PU administration results in shorter injectable times in this study, which is also a suitable injectable time for operation. If needed, further improvement of injectability could be achieved by adjusting the proportion of IPDI and PTMEG to obtain high NCO peaks in Part A. Flexible and designed components are good for different clinical applications, either in bone or in tooth repair.

Injectable materials constructed a solid structure during setting process. The interior structure of the composites affected the formation of the chemical network, which subsequently affected the macroscopic properties. Here, we explored the formation rate of the cross-linking structure by testing the gel content and swelling behavior of PUs; greater degrees of swelling resulted in lowered cross-linking density. The data demonstrated that cross-linking increased significantly with higher contents of n-HA (Table 2). Intermolecular cross-linking provides fibrillar matrices with various mechanical properties for PUs. It was shown that the increase of the cross-linking density led to a more stable network system, which is consistent with the compressive strength value. On the other hand, the increase of the inorganic phase is also a vitally important factor for better compressive strength. The compressive strength of the n-HA-incorporated PUs (3.8 MPa) is considerably higher than that of previous studies, which reported a compressive strength of 0.7 MPa for injectable polymeric carriers [9] and 0.1 MPa for injectable hydrogels [57]. The nano-needle, crystal-shaped HA particles are similar to rigid and short nanofibers (Star et al. [50], which can form stable uniform microstructures with PU substrates and improve the mechanical properties of PU composites. The reaction between n-HA and PUs also enhanced the bonding interface and improved the mechanical properties of the composites. In addition to these factors, the mechanical properties are also strongly affected by the degree of cross-linking obtained during the curing process discussed above.

The surface properties of PUs can significantly influence their performance. The contact angle drops to approximately 72° with the incorporation of n-HA. It was reported that surface wetting behavior plays an important role in the biomaterial interface, modulating both protein adsorption and cell adhesion [4]. The wettability of the PUs in this study was assessed by the contact angle. As expected, the high hydrophilic surface of PUs with the addition of n-HA rendered better hydrophilic action, as reflected by the contact angle of about a 10° decline. This is because n-HA has more ionizable groups, and these lead to stronger hydrogen bonding interactions. Laschke et al. [27]. also reported that the incorporation of HA particles into PU scaffolds generated an increase in superficial oxygen atoms and consequently enhanced the surface energy. The contact angle of natural bone was closed at 70° [49], so it is a suitable injectable adhesive as bone filling. The similar hydrophilic surfaces of PUs with n-HA are more conductive to cell adhesion and growth.

4.2 Antibacterial properties

To further confirm the release characteristics of Ag^+, the release rates were calculated as an indicator (as per Fig. 4a–b). By observing the antimicrobial mechanisms, it was clear that the soluble silver (+ 1) that dissolved from salts presented as the proper antibacterial agent, while the silver nanoparticle (Ag^0) acted as a reservoir [41]. The action of monovalent silver ions is that they possess a very high affinity for organic amines, phosphates, and thiols (most notably), with which they form a quasi-covalent bone [5]. When put in contact with bacteria, Ag^+ species tend to inactivate biological systems by forming an irreversible adduct with them. Basically, the solubility of silver (+ 1) phosphate (Ag_3PO_4) is 6.5 mg/L higher than that of Ag_2S (160 µg/L) and AgCl (1.9 mg/L). Thus, Ag_3PO_4 has been chosen as the antibacterial agent in the PU system. The rapid release rate in the initial period renders PUs as ideal candidates for preventing infection following their implantation and for treating acute inflammation after surgery. In fact, the steady and sustained release in later period makes PUs suitable for long-term antibacterial process. To investigate the application possibility of this injectable adhesive, the antibacterial effects and cytocompatibility were discussed in the following sections.

The results of the antibacterial tests showed that the silver-incorporated PUs had remarkably enhanced bactericidal properties towards *S. aureus*. The bactericidal ratio results revealed that the majority of *S. aureus* were killed after 24 h' incubation for PU30-1 s and PU30-3 s, as shown in Fig. 4c. Further, the 3 wt% Ag_3PO_4 showed the greatest antibacterial effects; similar results are shown in the SEM photos (Fig. 4e). This is because the PUs were immersed in the bacterial suspension; Ag^+ spread everywhere in the suspension and killed as many bacteria as possible. Similar results also demonstrated that silver cements have excellent-antibacterial properties against multiresistant bacteria on *S. epidermidis* (MRSE), *S. aureus* (MRSA), and *S. mutans*(ATCC), among others [8, 53]. However, *S. aureus*, as used in this study, represented a typical microorganism that could come into contact with implants. If necessary, the effect of the silver-incorporated PUs on other bacterial strains will be evaluated depending on the field of application. By comparing the area of the inhibition zone, we found that there were no significant differences observed between PU30-1 and PU30-3 against *S. aureus*. This was probably caused by the tardive extraction of silver ions on an agar plate. The release of Ag^+ on agar is dominated by diffusion rather than by silver content. Although the precise mechanisms for the inhibition of silver are still unclear, three possible hypotheses by the aqueous Ag^+ have been proposed: (1) interference with electron transport—in this way, Ag^+ can react with the essential protein complexes of bacterial electron transport chains exposed to the cell exterior and result in their deactivation [14]. (2) Binding to DNA—it has been reported that silver ions can inhibit DNA synthesis by directly binding on the bacterial DNA and preventing bacterial replication [3]. (3) Interaction with the cell components–it is generally believed that Ag^+ interfered with the metabolism of the bacteria, thus inhibiting its growth. Heavy metals react with proteins by combining the thiol (SH) groups, which leads to the inactivation of proteins [14]. The three possible hypotheses explained the broad antibacterial spectrum of Ag. Further, the multi-antimicrobial mechanism ensured protein denaturation, even leading to bacterial death.

4.3 Cytocompatibility in vitro

The cell cytotoxicity results suggested that low Ag_3PO_4concentrations (1 wt%) in PUs did not significantly affect cell proliferation. However, excessive Ag_3PO_4concentrations (3 wt%) led to poor cellular viability. These results are consistent with the Ag^+ release curve. The concentration of Ag^+ of PU30-3 (3 wt% Ag_3PO_4) had an effect on the agent's antimicrobial properties, but it inhibited cell growth, while the relatively low concentration of Ag^+ of PU30-1 (1 wt% Ag_3PO_4) retained high antibacterial activity and cytocompatibility. There are other reports suggesting that Ag_3PO_4 (1%) incorporated bone cement combines good antibacterial properties in the absence of cytotoxicity [3, 17]. The results of live/dead staining and cell adhesion in vitro preliminarily demonstrated that the PUs with 1 wt% Ag_3PO_4provided an optimal environment for cell adhesion, spreading, and proliferation, as compared to the black control groups. Furthermore, the beneficial effects of n-HA on osteogenic differentiation were confirmed herein. Increased ALP and OCN activity were observed on n-HA-incorporated PUs for the MSC cells after 14 and 21 days of culture. Furthermore, the ALP activity increased after increasing the n-HA ratio in PUs. The osteoconductive nature of n-HA resulted in higher ALP production at early differentiation stage and to OCN expression at later stage. Similar results have been observed by other studies on n-HA-added polymers.

From the above, we confirm that a nanocomposite adhesive system was fabricated by combining the cytocompatibility and antibacterial activities of n-HA/Ag_3PO_4/PU. Additionally, a conversion rate of over 90% was achieved for n-HA-incorporated PU adhesives according to the FTIR results. When examining the materials, the incorporation of n-HA not only improved the compressive strength substantially, but it also provided a superior wettability surface for PUs. Most importantly, the combination of the cytocompatibility and antibacterial properties for 1 wt% Ag_3PO_4 and 30 wt% n-HA established the n-HA/Ag_3PO_4/PU system as a

better candidate for injectable adhesives. Further biomolecules and animal evaluations have been tested based on the optimized characteristics of PUs.

5 Conclusion

An injectable PU system incorporating beneficial constituents of n-HA and Ag_3PO_4 have been developed for bone and tooth filling. All PU adhesives can achieve a high conversion rate in a short time; however, the incorporation of n-HA particles is the main effect of the material properties. The mechanisms and kinetics showed that the bonding reaction between the OH groups of the n-HA and NCO groups of PU, together with the system's higher cross-linking density, significantly accelerated the polymerization process with more inorganic filling content. Herein, the injectability and setting times, as well as the surface wettability of the PUs decreased, but the compressive strength and osteogenic differentiation factors significantly increased after increasing the n-HA content. Meanwhile, the incorporation of Ag_3PO_4 showed excellent and continual antibacterial activities to *S. aureus*, and PUs with 1 wt% Ag_3PO_4 expressed good cytocompatibility. Thus, the proper proportion of n-HA/Ag_3PO_4/PU could be adopted as a potential injectable system served for clinical adhesives.

Acknowledgements This work is supported by National Key Research and Development Program of China (2017YFC1104303/2017YFC1104300) and the China NSFC project (No. 31670965). We would like to thank Jiqiu Wen (Analytical & Testing Center of Sichuan University) for his help of XRD spectra.

Compliance with ethical standards

Conflicts of interest On behalf of all authors, the corresponding author states that there is no conflict of interest.

References

1. Adhikari R, Gunatillake PA, Griffiths I et al (2008) Biodegradable injectable polyurethanes: synthesis and evaluation for orthopaedic applications. Biomaterials 29:3762–3770. https://doi.org/10.1016/j.biomaterials.2008.06.021
2. Adolph EJ, Hafeman AE, Davidson JM et al (2012) Injectable polyurethane composite scaffolds delay wound contraction and support cellular infiltration and remodeling in rat excisional wounds. J Biomed Mater Res A 100:450–461. https://doi.org/10.1002/jbm.a.33266
3. Alt V, Bechert T, Steinrucke P et al (2004) An in vitro assessment of the antibacterial properties and cytotoxicity of nanoparticulate silver bone cement. Biomaterials 25:4383–4391. https://doi.org/10.1016/j.biomaterials.2003.10.078
4. Anselme K, Bigerelle M, Noel B et al (2000) Qualitative and quantitative study of human osteoblast adhesion on materials with various surface roughnesses. J Biomed Mater Res 49:155–166. https://doi.org/10.1002/(SICI)1097-4636(200002)49:23.3.CO;2-A
5. Barngrover BM, Aikens CM (2011) Incremental binding energies of gold(I) and silver(I) thiolate clusters. J Phys Chem 115:11818–11823. https://doi.org/10.1021/jp2061893
6. Bonzani IC, Adhikari R, Houshyar S et al (2007) Synthesis of two-component injectable polyurethanes for bone tissue engineering. Biomaterials 28:423–433. https://doi.org/10.1016/j.biomaterials.2006.08.026
7. Cai B, Zou Q, Zuo Y et al (2016) Fabrication and cell viability of injectable n-HA/chitosan composite microspheres for bone tissue engineering. RSC Adv 6:85735–85744. https://doi.org/10.1039/C6RA06594E
8. Chen W, Liu Y, Courtney HS et al (2006) In vitro anti-bacterial and biological properties of magnetron co-sputtered silver-containing hydroxyapatite coating. Biomaterials 27:5512–5517. https://doi.org/10.1016/j.biomaterials.2006.07.003
9. Cui X, Zhang Y, Wang H et al (2015) An injectable borate bioactive glass cement for bone repair: preparation, bioactivity and setting mechanism. J Non-cryst Solids 432:150–157. https://doi.org/10.1016/j.jnoncrysol.2015.06.001
10. Dallas P, Sharma VK, Zboril R (2011) Silver polymeric nanocomposites as advanced antimicrobial agents: classification, synthetic paths, applications, and perspectives. Adv Colloid Interface Sci 166:119–135. https://doi.org/10.1016/j.cis.2011.05.008
11. Ding Z, Li H, Wei J et al (2018) Developing a novel magnesium glycerophosphate/silicate-based organic-inorganic composite cement for bone repair. Mater Sci Eng C-Mater 87:104–111. https://doi.org/10.1016/j.msec.2018.03.001
12. Dumas JE, Prieto EM, Zienkiewicz KJ et al (2014) Balancing the rates of new bone formation and polymer degradation enhances healing of weight-bearing allograft/polyurethane composites in rabbit femoral defects. Tissue Eng Part A 20:115–429. https://doi.org/10.1089/ten.TEA.2012.0762
13. Ekambaram M, Yiu CKY, Matinlinna JP (2015) Bonding of adhesive resin to intraradicular dentine: a review of the literature. Int J Adhes Adhes 60:92–103. https://doi.org/10.1016/j.ijadhadh.2015.04.003
14. El-Kady AM, Ali AF, Rizk RA et al (2012) Synthesis, characterization and microbiological response of silver doped bioactive glass nanoparticles. Ceram Int 38:177–188. https://doi.org/10.1016/j.ceramint.2011.05.158
15. Farrar DF (2012) Bone adhesives for trauma surgery: a review of challenges and developments. Int J Adhes Adhes 33:89–97. https://doi.org/10.1016/j.ijadhadh.2011.11.009
16. Fedak PWM, Kieser TM, Maitland AM et al (2011) Adhesive-enhanced sternal closure to improve postoperative functional recovery: a pilot, randomized controlled trial. Ann Thorac Surg 92:1444–1450. https://doi.org/10.1016/j.athoracsur.2011.05.014
17. Fullenkamp DE, Rivera JG, Gong YK et al (2012) Mussel-inspired silver-releasing antibacterial hydrogels. Biomaterials 33:3783–3791. https://doi.org/10.1016/j.biomaterials.2012.02.027
18. Heitman EP, Joyce AP, Rd MPJ et al (2008) An in vitro evaluation of the growth of human periodontal ligament fibroblasts after exposure to a methacrylate-based endodontic sealer. J Endod 34:186–189. https://doi.org/10.1016/j.joen.2007.10.018

19. Hsieh KH, Liao KH, Lai EH et al (2008) A novel polyurethane-based root canal-obturation material and urethane acrylate-based root canal sealer–part I: synthesis and evaluation of mechanical and thermal properties. J Endod 34:303–305. https://doi.org/10.1016/j.joen.2007.12.006
20. Hu X, Shen H, Yang F et al (2014) Modified composite microspheres of hydroxyapatite and poly(lactide-co-glycolide) as an injectable scaffold. Appl Surf Sci 292:764–772. https://doi.org/10.1016/j.apsusc.2013.12.045
21. Huang Y, Zhang X, Wu A et al (2016) An injectable nano-hydroxyapatite (n-HA)/glycol chitosan (G-CS)/hyaluronic acid (HyA) composite hydrogel for bone tissue engineering. RSC Adv 6:33529–33536. https://doi.org/10.1039/C5RA26160K
22. Jaime CC, John KC, Lin A (2005) Antimicrobial behavior of polyelectrolyte multilayer films containing cetrimide and silver. Biomacromol 6:1149–1153. https://doi.org/10.1021/bm049528c
23. Jiang J, Li L, Li K et al (2016) Antibacterial nano-hydroxyapatite/polyurethane composite scaffolds with silver phosphate particles for bone regeneration. J Biomater Sci-Polym Edit 27:1584–1598. https://doi.org/10.1080/09205063.2016.1221699
24. Jones DM (1981) Manual of methods for general bacteriology. J Clin Pathol 34:1069. https://doi.org/10.1136/jcp.34.9.1069-c
25. Khairoun I, Boltong MG, Driessens FC et al (1998) Some factors controlling the injectability of calcium phosphate bone cements. J Mater Sci Mater Med 9:425–428. https://doi.org/10.1023/A:1008811215655
26. Lakhkar NJ, Park JH, Mordan NJ et al (2012) Titanium phosphate glass microspheres for bone tissue engineering. Acta Biomater 8:4181–4190. https://doi.org/10.1016/j.actbio.2012.07.023
27. Laschke MW, Strohe A, Menger MD et al (2010) In vitro and in vivo evaluation of a novel nanosize hydroxyapatite particles/poly(ester-urethane) composite scaffold for bone tissue engineering. Acta Biomater 6:2020–2027. https://doi.org/10.1016/j.actbio.2009.12.004
28. Lee BS, Wang CY, Fang YY et al (2011) A novel urethane acrylate-based root canal sealer with improved degree of conversion, cytotoxicity, bond strengths, solubility, and dimensional stability. J Endod 37:246–249. https://doi.org/10.1016/j.joen.2010.11.008
29. Lee Y, Bae JW, Oh DH et al (2013) In situ forming gelatin-based tissue adhesives and their phenolic content-driven properties. J Mater Chem B 1:2407–2414. https://doi.org/10.1039/c3tb00578j
30. Li S, Vatanparast R, Lemmetyinen H (2000) Cross-linking kinetics and swelling behaviour of aliphatic polyurethane. Polymer 41:5571–5576. https://doi.org/10.1016/S0032-3861(99)00785-5
31. Li YW, Leong JC, Lu WW et al (2000) A novel injectable bioactive bone cement for spinal surgery: a developmental and preclinical study. J Biomed Mater Res A 52:164–170. https://doi.org/10.1002/1097-4636(200010)52:1%3c164:AID-JBM21%3e3.0.CO;2-R
32. Li L, Zuo Y, Zou Q et al (2015) Hierarchical structure and mechanical improvement of an n-HA/GCO-PU composite scaffold for bone regeneration. ACS Appl Mater Interface 7:22618–22629. https://doi.org/10.1021/acsami.5b07327
33. Li K, Zuo Y, Zou Q et al (2016) Synthesis and characterization of injectable nano-hydroxyapatite/polyurethane composite cement effective formulations for management of osteoporosis. J Nanosci Nanotechnol 16:12407–12417. https://doi.org/10.1166/jnn.2016.13763
34. Lodiene G, Morisbak E, Bruzell E et al (2008) Toxicity evaluation of root canal sealers in vitro. Int Endod J 41:72–77. https://doi.org/10.1111/j.1365-2591.2007.01321.x
35. Massazza G, Bistolfi A, Verné E et al (2015) Antibiotics and cements for the prevention of biofilm-associated infections. Biomater Med Device-Assoc Infect 9:185–197. https://doi.org/10.1533/9780857097224.2.185
36. Mo A, Liao J, Xu W et al (2008) Preparation and antibacterial effect of silver-hydroxyapatite/titania nanocomposite thin film on titanium. Appl Surf Sci 255:435–438. https://doi.org/10.1016/j.apsusc.2008.06.083
37. Muñoz-Bonilla A, Fernández-García M (2012) Polymeric materials with antimicrobial activity. Prog Polym Sci 37:281–339. https://doi.org/10.1016/j.progpolymsci.2011.08.005
38. Neel EAA, Young AM (2013) Antibacterial adhesives for bone and tooth repair.Young. Join Assem Med Mater Devices 17:491–513. https://doi.org/10.1533/9780857096425.4.491
39. Neel EAA, Young AM (2013) 17-Antibacterial adhesives for bone and tooth repair. Join Assem Med Mater Devices 17:491–513. https://doi.org/10.1533/9780857096425.4.491
40. Ohashi S, Saku S, Yamamoto K (2004) Antibacterial activity of silver inorganic agent YDA filler. J Oral Rehabil 31:364–367. https://doi.org/10.1111/j.1365-2842.2004.01200.x
41. Ouay BL, Stellacci F (2015) Antibacterial activity of silver nanoparticles: a surface science insight. Nano Today 10:339–354. https://doi.org/10.1016/j.nantod.2015.04.002
42. Page JM, Prieto EM, Dumas JE et al (2012) Biocompatibility and chemical reaction kinetics of injectable, settable polyurethane/allograft bone biocomposites. Acta Biomater 8:4405–4416. https://doi.org/10.1016/j.actbio.2012.07.03
43. Rai M, Yadav A, Gade A (2009) Silver nanoparticles as a new generation of antimicrobials. Biotechnol Adv 27:76–83. https://doi.org/10.1016/j.cis.2008.09.002
44. Sariibrahimoglu K, Wolke JG, Leeuwenburgh SC et al (2014) Injectable biphasic calcium phosphate cements as a potential bone substitute. J Biomed Mater Res B 102:415–422. https://doi.org/10.1002/jbm.b.33018
45. Sartori S, Chiono V, Tonda-Turo C et al (2014) Biomimetic polyurethanes in nano and regenerative medicine. J Mater Chem B 2:5128–5144. https://doi.org/10.1039/C4TB00525B
46. Sharma VK, Yngard RA, Lin Y (2009) Silver nanoparticles: green synthesis and their antimicrobial activities. Adv Colloid Interface Sci 145:83–96. https://doi.org/10.1016/j.cis.2008.09.002
47. Shi Z, Neoh KG, Kang ET et al (2006) Antibacterial and mechanical properties of bone cement impregnated with chitosan nanoparticles. Biomaterials 27:2440–2449. https://doi.org/10.1016/j.biomaterials.2005.11.036
48. Slawson RM, Lee H, Trevors JT (1990) Bacterial interactions with silver. Biol Metals 3:151–154. https://doi.org/10.1007/BF01140573
49. Song JM, Oh SH, Kim JS et al (2005) Effects of compositional inhomogeneity on the mechanical properties and morphology of styrene-co-methacrylate random ionomer mixtures. Polymer 46:12393–12400. https://doi.org/10.1016/j.polymer.2005.10.124
50. Star A, Stoddart JF, Steuerman D et al (2001) Preparation and properties of polymer-wrapped single-walled carbon nanotubes. Angew Chem Int Ed 40:1721–1725. https://doi.org/10.1002/1521-3773(20010504)40:9%3c1721:AID-ANIE17210%3e3.0.CO;2-F
51. Sun B, Zuo Y, Li J et al (2013) High conversion self-curing sealer based on a novel injectable polyurethane system for root canal filling. Mater Sci Eng C Mater Biol Appl 33:3138–3145. https://doi.org/10.1016/j.msec.2013.03.014
52. Wang L, Heuchel M, Fang L et al (2012) Influence of a polyester coating of magnetic nanoparticles on magnetic heating behavior of shape-memory polymer-based composites. J Appl Biomater Funct 10:203–209. https://doi.org/10.5301/JABFM.2012.10293
53. Wang J, Zuo Y, Zhao M et al (2015) Physicochemical and biological properties of a novel injectable polyurethane system for root canal filling. Int J Nanomed 10:697–709. https://doi.org/10.2147/IJN.S74025
54. Wang Y, Li P, Xiang P et al (2016) Electrospun polyurethane/keratin/AgNPbiocomposite mats for biocompatible and antibacterial

wound dressings. J Mater Chem B 4:635–648. https://doi.org/10.1039/C5TB02358K
55. Wu X, Li J, Wang L et al (2010) The release properties of silver ions from Ag-nHA/TiO_2/PA66 antimicrobial composite scaffolds. Biomed Mater 5:044105–044112. https://doi.org/10.1088/1748-6041/5/4/044105
56. Xu X, He L, Zhu B et al (2017) Advances in polymeric materials for dental applications. Polym Chem 8:807–823. https://doi.org/10.1039/C6PY01957A
57. Zhao L, Weir MD, Xu HH (2010) An injectable calcium phosphate-alginate hydrogel-umbilical cord mesenchymal stem cell paste for bone tissue engineering. Chin J Joint Surg 31:6502–6510. https://doi.org/10.1016/j.biomaterials.2010.05.017
58. Zou Q, Li Y, Zhang L et al (2009) Characterization and cytocompatibility of nano-hydroxyapatite/chitosan bone cement with the addition of calcium salts. J Biomed Mater Res B 90B:156–164. https://doi.org/10.1002/jbm.b.31267